ELSEVIER

Journal of Biomechanics 38 (2005) 1093–1105

JOURNAL OF BIOMECHANICS

www.elsevier.com/locate/jbiomech
www.JBiomech.com

High rate shear strain of three-dimensional neural cell cultures: a new in vitro traumatic brain injury model

Michelle C. LaPlaca[a,*], D. Kacy Cullen[a], Justin J. McLoughlin[b], Robert S. Cargill II[b,1]

[a] Coulter Department of Biomedical Engineering, Georgia Institute of Technology, 313 Ferst Drive, Atlanta GA, USA
[b] Woodruff School of Mechanical Engineering, Georgia Institute of Technology, 801 Ferst Drive, Atlanta GA, USA

Accepted 20 May 2004

Abstract

The fidelity of cell culture simulations of traumatic brain injury (TBI) that yield tolerance and mechanistic information relies on both the cellular models and mechanical insult parameters. We have designed and characterized an electro-mechanical cell shearing device in order to produce a controlled high strain rate injury (up to 0.50 strain, 30 s^{-1} strain rate) that deforms three-dimensional (3-D) neural cultures (neurons or astrocytes in an extracellular matrix scaffold). Theoretical analysis revealed that these parameters generate a heterogeneous 3-D strain field throughout the cultures that is dependent on initial cell orientation within the matrix, resulting in various combinations of normal and shear strain. The ability to create a linear shear strain field over a range of input parameters was verified by tracking fluorescent microbeads in an acellular matrix during maximal displacement for a range of strains and strain rates. In addition, cell death was demonstrated in rat cortical astrocytes and neurons in response to high rate, high magnitude shear strain. Furthermore, cell response within the 3-D neuronal cultures depended on orientation, with higher predicted shear strain correlating with an increased loss of neurites, indicating that culture configuration may be an important factor in the mechanical, and hence cellular, response to traumatic insults. Collectively, these results suggest that differential responses exist within a 3-D culture subjected to mechanical insult, perhaps mimicking the in vivo environment, and that this new model can be used to investigate the complex cellular mechanisms associated with TBI.

Keywords: Strain rate; 3-D; Astrocyte; Neuron; Traumatic injury; Cell mechanics

1. Introduction

Traumatic brain injury (TBI) is a severe health and socioeconomic problem, for which there are few effective clinical treatments (Roberts et al., 1998). TBI results from mechanical loading to the head and therefore models that seek to reveal injury mechanisms should accurately simulate the related biomechanics. Traumatic loading to the head can involve several components, including contact and/or inertial loading (Gennarelli, 1993). The severity of neurological disability depends on the initial insult and the ensuing cellular cascades, which may be complex and persistent.

Although in vivo studies model the systemic and behavioral deficits of TBI, in vitro approaches provide a powerful framework for investigating isolated mechanisms. Cellular models range from transection (Gross et al., 1983; Lucas et al., 1985; Mukhin et al., 1996; Regan and Choi, 1994; Tecoma et al., 1989) and compression models (Balentine et al., 1988; Murphy and Horrocks, 1993; Shepard et al., 1991; Wallis and Panizzon, 1995) (contact loading) to more complex stretching and acceleration devices (Cargill and Thibault, 1996; Ellis et al., 1995; Geddes and Cargill, 2001; LaPlaca and Thibault, 1997) (inertial loading). Inertial loading has been correlated with severe, diffuse brain injury that is attributed to stretching neural components (Gennarelli, 1993; Margulies and Thibault, 1992; Ommaya et al., 1994). The spatial and temporal patterns

*Corresponding author. Laboratory for Neuroengineering, Georgia Institute of Technology, 313 Ferst Drive, Atlanta, GA 30332-0535, USA. Tel.: +1-404-385-0629; fax: +1-404-385-5044.
E-mail address: michelle.laplaca@bme.gatech.edu (M.C. LaPlaca).
[1] Present address: Exponent Failure Analysis Associates, 3401 Market Street, Suite 300, Philadelphia, PA 19104, USA

0021-9290/$ - see front matter © 2004 Elsevier Ltd. All rights reserved.
doi:10.1016/j.jbiomech.2004.05.032

of strain associated with inertial loading are the basis for several in vivo and in vitro injury models that apply large strains (see Gennarelli, 1994; Morrison et al., 1998a, b for reviews). In addition to the strain magnitude, the tensorial nature of strain is a determining factor in tissue outcome. In fact, the primary mode of failure in neural tissue is shear (Holburn, 1943; Shuck and Advani, 1972). Models that employ rapid mechanical deformation often exhibit a strain- and/or strain rate-dependent injury, thus substantiating the clinical observation that angular acceleration and injury severity are causally related.

Planar (2-D) cultures differ markedly from the three-dimensional (3-D) cytoarchitecture of the brain. Cell behaviors of 2-D versus 3-D cell configurations have shown that 3-D cultures more closely resemble those of native tissue (e.g., osteoblastic cells (Granet et al., 1998), hepatocytes (Takeshita et al., 1998), breast cells (Wang et al., 1998), and neural cells (Fawcett et al., 1989, 1995)), suggesting that 3-D models may yield more accurate secondary responses. Cells cultured in 2-D have different cell–cell and cell–matrix interactions than 3-D cultures (Cukierman et al., 2001, 2002; Gumbiner and Yamada, 1995; Schmeichel and Bissell, 2003; Yamada et al., 2003), potentially impacting mechanotransduction associated with traumatic insults. In this context, brain slices (ranging in thickness from 200 to 500 μm) have been utilized to determine molecular responses to injury (Morrison et al., 1998a, b; Sieg et al., 1999; Wallis and Panizzon, 1995). Although slice models are invaluable to in vitro investigations, the ability to control cell types, ratio of cell types, and extracellular components—factors that may be important to the injury response—is limited.

A device that incorporates the features of 3-D cell cultures under conditions of simple shear strain would be a significant addition to the repertoire of cell injury devices in the study of TBI. To this end, we have developed a 3-D cell shearing device (CSD) that delivers a prescribed shear strain to 3-D cell cultures. The strain is controlled by a closed loop system, ensuring precise and repeatable deformation. The objectives of the current study are (1) to analytically describe the 3-D strain field for a range of shear displacement angles, (2) to measure the strain field throughout a 3-D gel configuration, and (3) to test the ability of the system to induce cell injury in 3-D neural cultures (neonatal rat cortical astrocytes and embryonic rat cortical neurons).

2. Methods

2.1. Three-dimensional cell shearing device (3-D CSD)

The primary design goal for the 3-D CSD was to have control over the magnitude and rate of displacement. The 3-D CSD has two major components: the cell chamber and the actuator/control system (Fig. 1a). The cell chamber is designed to contain enough cells for molecular analyses in a 3-D configuration. The actuator/control system develops shear strains up to 0.50 (shear angle up to 45°) at rates from 1 to 30 s^{-1} in order to simulate the spatial and temporal strain patterns associated with inertial TBI (Margulies and Thibault, 1992).

2.1.1. Cell chamber

The cell chamber is comprised of the cell reservoir and the top plate (Fig. 1b). The cell reservoir is a rectangular polycarbonate well with a glass floor (no. $1\frac{1}{2}$ coverslip). Parallel shoulders were machined into the upper surface of the two long sides of the polycarbonate walls to provide proper alignment and constrain motion of the top plate to a single axis. The 3-D cultures (two per reservoir) are confined within an elastomer mold composed of Sylgard 184 and 186 (Dow Corning; Midland, MI), which were mixed 1:1 (w/w) and cast to the desired thickness. For culture containment, two cutouts (inner dimensions of each, 10 mm × 10 mm or 15 mm × 15 mm) were made with a razor punch. Throughout experimentation, the mold adhered firmly to the bottom glass coverslip without any movement. The top plate is composed of a polycarbonate body with two C-shaped protrusions on the bottom surface. The C-shaped protrusions act as struts to transfer the transverse motion of the top plate to the cell culture via a porous, hydrophilic polyethylene filter (15–45 μm pore size; Porex Corp; Atlanta, GA) which is attached to the C-shaped protrusions on the topside and directly to the cell culture on the bottomside. The porous filter permits transfer of nutrients and waste. The top plate is attached to the linear actuator by a polycarbonate extension plate that is mounted to a linear bearing system (Thomson Bearings; Port Washington, NY).

2.1.2. Actuator and closed loop motion control system

The 3-D CSD generates a dynamic shear strain by the linear motion of the top plate with respect to the cell reservoir (Fig. 1c) via a linear voice coil actuator (BEI Kimco; San Marcos, CA) and a closed loop control system consisting of a proportional-integral-derivative (PID) controller (Feedback Inc.; Hillsborough, NC), an amplifier (Advanced Motion Controls; Camarillo, CA), and a differential variable reluctance transducer (DVRT) (Microstrain; Burlington, VT). The linear actuator produces a rigid body translation of the top plate assembly using a function generator (Hewlett Packard; Palo Alto, CA). The input signal is the reference input to the PID controller and is compared internally to the actual displacement of the top plate provided by the DVRT. The closed loop controller produces a self-correcting signal to minimize the error

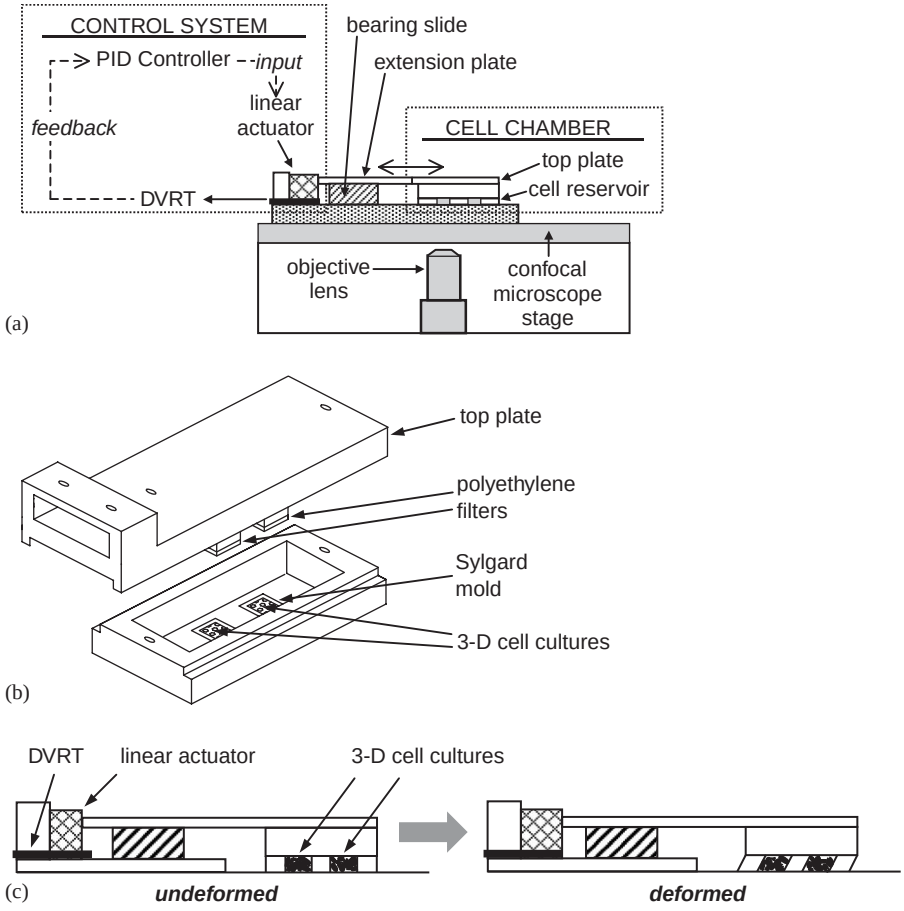

Fig. 1. 3-D Cell Shearing Device (3-D CSD) components. (a) A schematic representation of the 3-D CSD. The device can be mounted on a confocal microscope to obtain 3-D images before, during, and after mechanical deformation. A closed-loop control system (PID controller with feedback from a DVRT) governs a linear actuator, inducing motion of the cell chamber top plate (not to scale). (b) The cell chamber consists of a top plate with polyethylene filters to interface with the 3-D cell cultures. The top plate is mounted above the cell reservoirs and connected to the linear actuator to impart high rate deformation. (c) The horizontal motion of the linear actuator drives the displacement of the cell chamber top plate, inducing shear deformation in the Sylgard mold and matrix (with either cells or microbeads) (not to scale).

between the actual and desired position. PID control reduces steady-state error between the input signal and the motion of the top plate, eliminates possible oscillations in the response, and increases sensitivity of the system. A modification of the Ziegler–Nichols tuning method was used to set the initial values of the PID and subsequently to obtain an optimal range of PID settings.

2.1.3. Analysis

The 3-D strain field for a range of displacements was analyzed using a continuum mechanics approach. A neural cell was modeled as a line element and placed in various orientations. This kinematic analysis of the shear strain field in the 3-D CSD may aid in validating our experimental findings and lend insight into the mechanisms of shear-induced injury. The amount of neurite loss in injured neurons was then analyzed as a function of theoretical strains in the 3-D constructs to test the hypothesis that high shear strain fields will result in increased cell dysfunction.

2.2. Strain field characterization

The shear displacement field was validated using a 3-D acellular construct. Microbeads were embedded in Matrigel basement membrane matrix (Becton Dickinson; Bedford, MA) and tracked on an epifluorescent laser scanning confocal microscope (Zeiss LSM 510 UV). The testing sample was cast by mixing Matrigel and Dulbecco's Modified Eagle Media (DMEM) (1:1) with FluoSpheres carboxylate-modified microspheres (0.5 μm diameter, 9×10^6 beads/ml; Molecular Probes; Eugene, OR). The mixture was triturated and a sufficient amount to create 500 μm thick constructs was distributed into each mold and allowed to set for 4 h at 37°C. Three-dimensional constructs were subsequently mounted on the 3-D CSD. A symmetric trapezoidal reference function was generated for each of the following deformation profiles: strain 0.25, strain rate $1\,s^{-1}$, $n=4$; strain 0.25, strain rate $10\,s^{-1}$, $n=5$; strain 0.25, strain rate $20\,s^{-1}$, $n=4$; strain 0.50, strain rate $1\,s^{-1}$, $n=4$; strain 0.50, strain rate $10\,s^{-1}$, $n=3$;

strain 0.50, strain rate $20\,s^{-1}$, $n = 4$. A long dwell time (strain-and-hold) was used to allow the microscope to scan through multiple planes. Images from the confocal microscope were obtained for 20 planes (2 μm thickness) throughout the cultures. The relative positions of one to four beads for each plane were measured pre-strain and during maximum strain in order to calculate the displacement of each bead.

2.3. Cell culture

Astrocytes were harvested from postnatal day 1 rat pups. The pups were rapidly decapitated, and the cerebral hemispheres were placed in sterile Hank's Balanced Salt Solution (HBSS). The isolated cortices were minced and the tissue fragments were then digested in trypsin (0.25% + 1 mM EDTA) for 3–5 min at 37°C, followed by DNase I (0.15 mg/ml) treatment and gentle mechanical trituration. Cells were then centrifuged at 1000 rpm for 3 min, dispersed in DMEM/F12 with 10% fetal bovine serum (FBS), and plated in a flask. Neurons and microglia were mechanically detached at 24 and 72 h and the primary astrocyte culture (>95% type I astroctyes) was passaged upon reaching ~90% confluency. Astrocytes were used between passages 5 and 10 for plating in 3-D culture (see below).

Neurons were isolated from embryonic day 17 rat fetuses. Each fetus was removed by Caesarian section, rapidly decapitated, and the brains were removed. The cortices were isolated and digested in HBSS with trypsin (0.25% + 1 mM EDTA) at 37°C for 10 min. The trypsin-EDTA was then removed and the tissue was triturated in HBSS containing DNase I (0.15 mg/ml). The cells were centrifuged at 1000 rpm for 3 min and the cells were resuspended in neuronal plating medium (Neurobasal medium + 2% B27 + 500 μM L-glutamine) immediately prior to 3-D plating.

Cell chambers were autoclaved and the cell reservoirs were prepared by coating all sides in poly-L-lysine (0.0015%), facilitating Matrigel adsorption to the edge of the Sylgard mold and the bottom glass. Three-dimensional cultures were made by mixing suspended astrocytes (in DMEM/F12) or suspended neurons (in neuronal plating medium) with liquid Matrigel (1:1) and adding a sufficient volume to create 500 μm thick cultures (final cell densities of 1000 astrocytes/mm^3 or 5000 neurons/mm^3). Following Matrigel gelation at 37°C, medium was added to the cell reservoirs above the matrices (DMEM/F12 + 2% FBS for astrocyte cultures and neuronal plating medium for neuron cultures).

All procedures using animals conformed to guidelines set forth in the NIH Guide for the Care and Use of Laboratory Animals and were approved by the Georgia Tech Institutional Animal Care and Use Committee. All cell reagents were obtained from Invitrogen (Carlsbad, CA) or Sigma (St. Louis, MO) unless otherwise noted.

2.4. Cell deformation

Cells were mechanically loaded following mounting the cell reservoir within the 3-D CSD and attaching the top plate to the extension plate. Astrocyte cultures (2–3 days post 3-D plating) were either subjected to deformation in the 3-D CSD (strain 0.25, strain rate $1\,s^{-1}$, $n = 4$; strain 0.25, strain rate $20\,s^{-1}$, $n = 4$; strain 0.50, strain rate $1\,s^{-1}$, $n = 6$; strain 0.50, strain rate $20\,s^{-1}$, $n = 5$), placed into the device with the top plate (sham control, $n = 8$) or left undisturbed (naïve control, $n = 4$). Neuron cultures (7 days post 3-D plating) were deformed using the same protocol (strain 0.50, strain rate $20\,s^{-1}$, $n = 6$; strain 0.50, strain rate $30\,s^{-1}$, $n = 8$) or placed into the device with the top plate (sham control, $n = 6$) or left undisturbed (naïve control, $n = 4$). A symmetric trapezoidal pulse was employed with the following rise times (in ms): 250 (0.25, $1\,s^{-1}$), 500 (0.50, $1\,s^{-1}$), 12.5 (0.25, $20\,s^{-1}$), 25 (0.50, $20\,s^{-1}$), and 16.6 (0.50, $30\,s^{-1}$). After the deformation was applied, warm medium was added and the cultures were returned to the incubator until cell viability was assessed.

2.5. Cell viability and neurite orientation

Astrocyte and neuron survival was assessed using fluorescent probes (LIVE/DEAD Viability/Cytotoxicity Kit; Molecular Probes, Eugene, OR) and a confocal microscope (Zeiss). Twenty-four hours following deformation or sham conditions, cells were removed from the incubator, rinsed in phosphate buffered saline (PBS, pH 7.4) and incubated with 2 μM calcein AM and 4 μM ethidium homodimer (EthD-1) at 37°C for 30 min. After rinsing with PBS, confocal z-stacks were acquired across the thickness of the cultures. After deformation or sham conditions, the percent of viable cells and the distribution of neurites in viable neurons were assessed using the DSM Confocal Image Viewer (Zeiss). Live and dead cells were manually quantified through the thickness of the cultures. The number of neurites was determined at discrete orientation angles by rotating the viewing plane about the x_1-axis (corresponding to $\phi \in [-70°, 70°]$, see Results for definition) and manually quantifying the number of in-plane neurites that were greater than 10 μm in length. Three to five planes per orientation were counted; the field of view for each plane was 460 μm^2. The mean range of the number of neurites counted per plane was 25.1–64.2 for sham cultures and 5.0–20.9 for injured cultures. The number of neurites was then converted to percentage of neurites for each orientation in order to compare the injury to the sham conditions.

2.6. Statistical analysis

Regression analysis was performed on the measured bead displacements for each loading condition. The

slopes of the lines were then compared to theoretical values for simple shear strain using a t-test with $p<0.05$ considered statistically significant. Vertical bead displacement was measured (in the x_3 direction) and compared to total displacement in the x_2 direction. The percent of viable cells for each condition was analyzed using a two-way ANOVA (with strain and strain rate as independent variables and viability as the dependent variable) followed by a Tukey multiple comparison test. The percent distribution of neurites at various orientation angles was analyzed using a two-way repeated measures ANOVA with a Tukey multiple comparison test. A p-value <0.05 was considered significant.

3. Results

3.1. Kinematic analysis of 3-D strain field

It was hypothesized that the orientation of the cell within the 3-D matrix contributes to the strain transferred to the individual cells from bulk deformation. It was assumed that the overall shear strain field was homogeneous, isotropic, and the culture was incompressible. To describe the motion of points within the deformable matrix, a fixed reference frame in 3-D space was established where the Cartesian coordinates of a point were denoted by $\mathbf{x}=(x_1,x_2,x_3)$. The positions of any two adjacent reference points in an undeformed state were defined as $P:(x_1,x_2,x_3)$ and $Q:(x_1+\mathrm{d}x_1,x_2+\mathrm{d}x_2,x_3+\mathrm{d}x_3)$. The same two reference points were described in a deformed state as $\bar{P}:(\xi_1,\xi_2,\xi_3)$ and $\bar{Q}:(\xi_1+\mathrm{d}\xi_1,\xi_2+\mathrm{d}\xi_2,\xi_3+\mathrm{d}\xi_3)$. Thus, deformation was a one-to-one mapping from a reference configuration to a deformed configuration and can be represented by a continuous function $\xi_i=\xi_i(x_1,x_2,x_3,t)$ for $i=1,2,3$, where t denotes the time over which the deformation occurs. The initial angles between points projected into the x_3,x_2 plane and in the x_1,x_2 plane were denoted as ϕ and α, respectively (Fig. 2). The distance between two points was described as $\mathrm{d}S$ in an undeformed state and $\mathrm{d}\bar{S}$ in a deformed state. Accordingly, in reference to the initial configuration, the change in the squared distance between the two points becomes

$$(\mathrm{d}\bar{S})^2-(\mathrm{d}S)^2=2E_{ij}\,\mathrm{d}x_i\,\mathrm{d}x_j, \tag{1}$$

where E_{ij} is the Green's strain tensor. In the specific case of simple shear deformation, the location of a point in the deformed configuration may be described in terms of its initial location and the applied deformation:

$$\mathrm{d}\xi_1=\mathrm{d}x_1, \tag{2.1}$$

$$\mathrm{d}\xi_2=\mathrm{d}x_2+\mathrm{d}x_3\,tan(\gamma), \tag{2.2}$$

$$\mathrm{d}\xi_3=\mathrm{d}x_3, \tag{2.3}$$

where γ is the angle of shear deformation (Fig. 2) and vertical displacement is assumed to be zero. Accordingly, the components of the Green's strain tensor for this system are:

$$E_{ij}=\frac{1}{2}\begin{pmatrix}0&0&0\\0&0&\tan(\gamma)\\0&\tan(\gamma)&\tan^2(\gamma)\end{pmatrix}. \tag{3}$$

The Green's strain tensor is sufficient to describe the bulk deformation behavior of the cultures. However, we are interested in the state of strain relative to a local coordinate system fixed to a cell. These strains can be determined though coordinate transformations from the initial coordinate system to a coordinate system aligned with a particular unit vector of interest (representing, for example, a cellular process). A series of rotational transformations relate the initial strain tensor, $[E]$, and a transformed strain tensor, $[E']$, based on the transformation matrix $[R]$:

$$[E']=[R][E][R]^{\mathrm{T}}. \tag{4}$$

The transformation matrix was derived such that the new x_2-axis direction was aligned with the unit vector of interest through an initial rotation about the x_1-axis, followed by a space-fixed rotation about the original x_3-axis (Fig. 3). The angle of rotation about the x_1-axis, $\phi\in[-90^\circ,90^\circ]$, and the angle of rotation about the x_3-axis, $\alpha\in[-90^\circ,90^\circ]$, were derived based on the ratio of the distances between points of interest:

$$\tan(\phi)=\frac{\mathrm{d}x_3}{\mathrm{d}x_2}, \tag{5.1}$$

$$\tan(\alpha)=\frac{\mathrm{d}x_1}{\mathrm{d}x_2}. \tag{5.2}$$

Accordingly, the strain tensor as a function of initial orientation is

$$[E']=\frac{1}{2}\tan(\gamma)\begin{pmatrix}0&-\sin(\phi)\sin(\alpha)&-\cos(\phi)\sin(\alpha)\\-\sin(\phi)\sin(\alpha)&\sin(2\phi)\cos(\alpha)+\sin^2(\phi)\tan(\gamma)&\cos(2\phi)\cos(\alpha)+\frac{1}{2}\sin(2\phi)\tan(\gamma)\\-\cos(\phi)\sin(\alpha)&\cos(2\phi)\cos(\alpha)+\frac{1}{2}\sin(2\phi)\tan(\gamma)&-\sin(2\phi)\cos(\alpha)+\cos^2(\phi)\tan(\gamma)\end{pmatrix}. \tag{6}$$

The transformed Green's strain tensor represents the strain along vectors oriented at arbitrary angles with respect to the shear deformation field. Designation of the angles of orientation in the x_3,x_2 plane and in the x_1,x_2 plane (ϕ and α, respectively) is necessary to specify the strain along a vector of interest upon shear deformation. The normal strains along vectors at

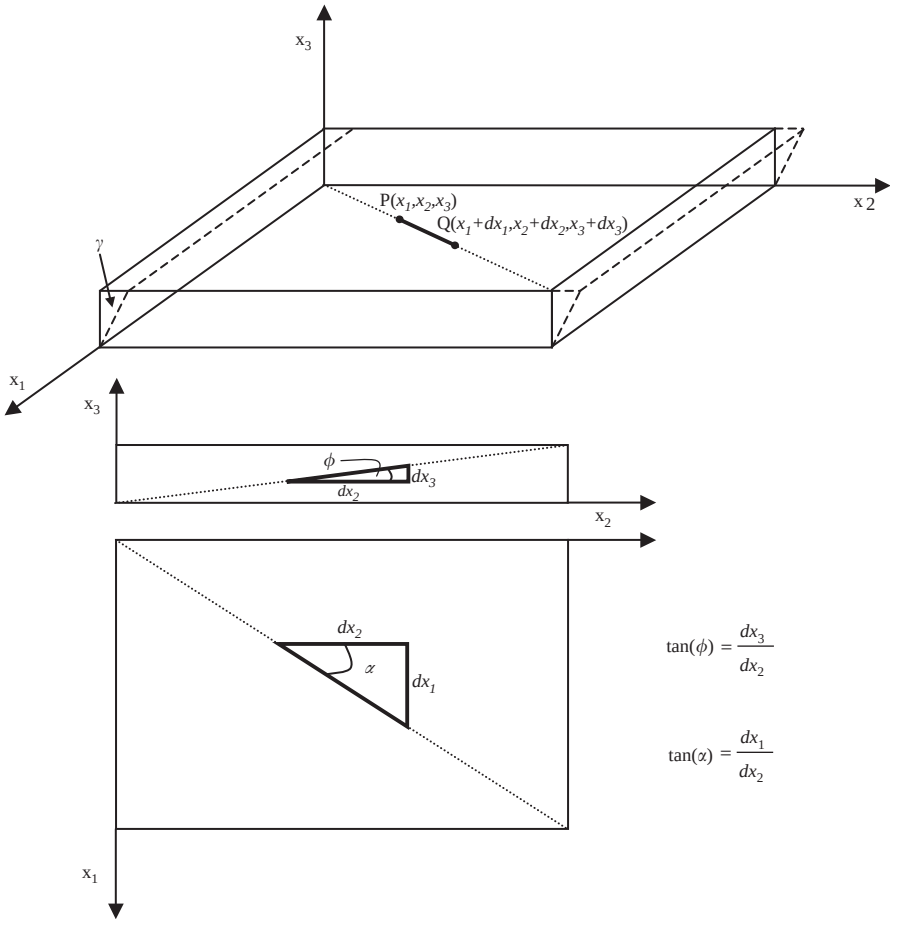

Fig. 2. Definitions of coordinate system used in theoretical strain analysis. The angles ϕ and α are defined as the angles between arbitrary points of reference projected to the x_3,x_2 plane and the x_1,x_2 plane, respectively. The distance along a fixed axis between these two arbitrary points is defined as dx_1 along the x_1-axis, dx_2 along the x_2-axis and dx_3 along the x_3-axis. The shear deformation of the cell-containing matrices (proportional to the angle γ) occurs in the x_3,x_2 plane.

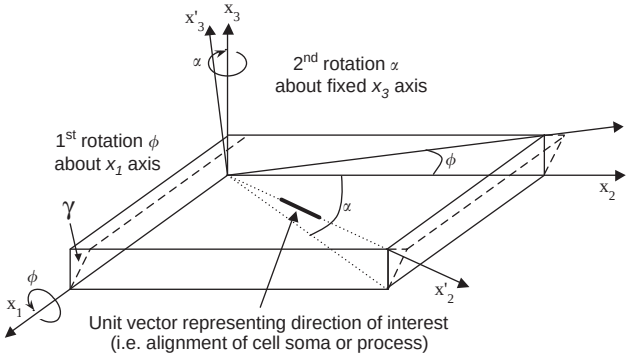

Fig. 3. Axis rotation descriptions. Axis rotations were used to align the x_2-axis with a direction of interest. The first rotation is about the x_1-axis by ϕ degrees. The second rotation is space-fixed about the x_3-axis by α degrees. This methodology permits the determination of the components of the Green's strain tensor specific for a cell process or soma at any orientation with respect to the strain field induced by the 3-D CSD.

various orientations are E'_{11} (lateral strain), E'_{22} (axial strain), and E'_{33} (vertical strain), of which E'_{22} and E'_{33} are plotted for the maximum shear angle ($\gamma = 45^\circ$) used in this study (Figs. 4a and b). The lateral strain was equal to zero regardless of the strain tensor orientation, thus motion between points within the x_1,x_2 plane maintains a fixed distance. Depending on the initial orientation, cellular components may undergo a wide range of axial and vertical strains causing both extension and compression. The shear strains along vectors at various orientations, E'_{12} (lateral-shear strain), E'_{13} (vertical-shear strain), and E'_{23} (axial-shear strain) are plotted at the maximum shear angle evaluated (Figs. 4c–e). Lateral and vertical-shear strains are non-zero only when the vector of interest is not parallel to the x_3,x_2 plane ($\alpha \neq 0$), and increase in magnitude as α increases. The deformation continuum that the cell-containing matrices undergo as the matrix is driven from an undeformed state ($\gamma = 0^\circ$) to a state of maximum deformation can result in: (1) continuous extension, (2) continuous compression, or (3) initial compression followed by extension. Furthermore, this cycle is reversed upon return to the initial, undeformed state.

This analysis demonstrates that the orientation of the principal axes changes with the magnitude of the shear

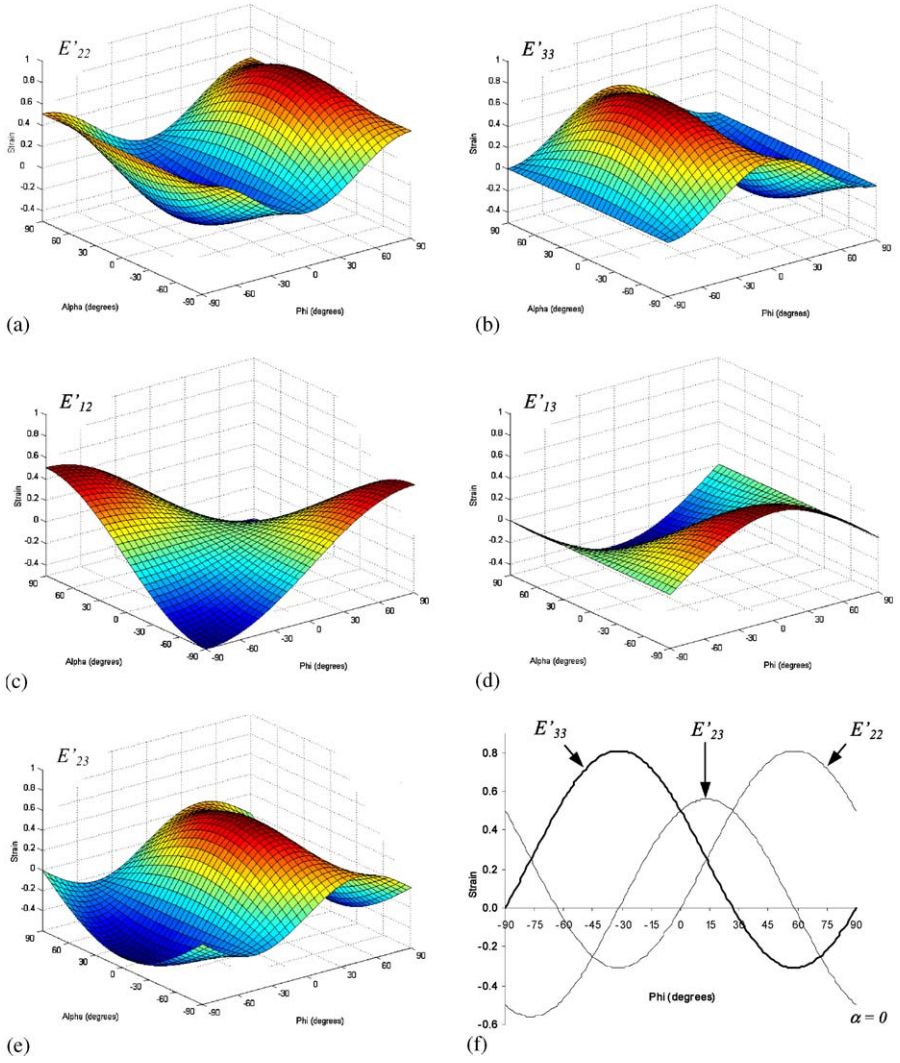

Fig. 4. Strain distribution for maximum shear ($\gamma = 45^\circ$). Elements of the Green's strain tensor as a function of the angles of orientation, ϕ and α, between a vector of interest and the x_3,x_2 and x_1,x_2 plane, respectively. (a) E'_{22} is the axial-normal strain, (b) E'_{33} is the vertical-normal strain, (c) E'_{12} is the lateral-shear strain, (d) E'_{13} is the vertical-shear strain, (e) E'_{23} is the axial-shear strain. E'_{11}, the lateral-normal strain, is zero independent of orientation. Depending on orientation, vectors of interest may experience a range of combinations of normal and shear strain with varying magnitudes and signs (signifying compression or extension) during loading with the 3-D CSD. (f) A plot of E'_{22}, E'_{33}, and E'_{23} when $\alpha = 0^\circ$ (all other strains are zero). The highest magnitude normal and shear strains occur at angles of orientation out of the horizontal plane.

deformation. The highest magnitude normal strains occur when

$$\phi = \tfrac{1}{2}\tan^{-1}\left[\frac{-2}{\tan(\gamma)}\right], \text{ and} \tag{7.1}$$

$$\alpha = 0. \tag{7.2}$$

The solutions to Eq. (7.1) yield the directions of principal normal strain in the initial coordinate system with the direction of maximum extension being located between 45° and 90°, and the direction of maximum compression being located between 0° and −45°. Within these ranges, as the shear angle increases, the directions of maximum extension and compression both increase (orthogonal principal normal axes rotate counterclockwise about the x_1-axis). Furthermore, the principal shear strains are located at axes 45° to the direction of the principal normal strains. These trends are depicted based on the shear strains utilized in this study (Table 1). This derivation was based on large deformation continuum mechanics and yielded results consistent with those previously attained for the orientation of the principal axis upon simple shear deformation (Ogden, 1984). Accordingly, with reference to the initial coordinate system, both the directions of principal shear strains and principal normal strains vary as functions of the shear angle.

This analysis suggests that the orientation for 3-D neural cells within a defined strain field may contribute to the heterogeneity of the strain at the cellular level.

Table 1
Orientation of the principal axes depends on shear angle

Bulk shear strain	Shear angle (γ)	Directions of principal normal strain	Directions of principal shear strain
0.25	26.6°	−38.0°, 52.0°	−83.0°, 7.0°
0.50	45.0°	−31.7°, 58.3°	−76.7°, 13.3°

The bulk shear strain refers to the overall shear strain for the cell-containing matrices based on a given shear angle. The axes of principal normal and shear strain were derived based on position in the initial, undeformed coordinate system and the angles describe values of ϕ (projected angle in the x_3, x_2 plane) when α (projected angle in the x_1, x_2 plane) is zero. As the shear angle increases, the direction of maximum extension increases towards 90° while the angle of maximum compression moves towards 0°. The directions of principal shear strain are located at axes 45° to the directions of principal normal strain.

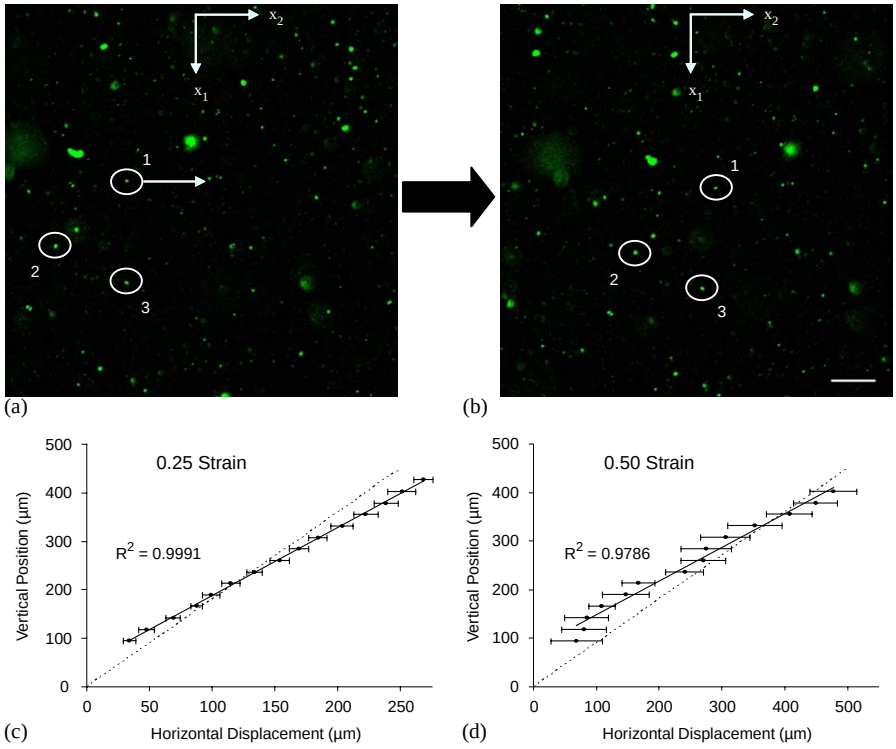

Fig. 5. Representative photomicrographs of microbead tracking. A single plane (a) before deformation and (b) during deformation with the 3-D CSD (scale bar = 50 μm). Bead displacements across the thickness of the gel from the bottom to the top (vertical displacements of 0 and 500 μm, respectively) were measured at maximum deformation. Measured displacements are presented as a mean value and SEM (data points with error bars and a best-fit solid line). The theoretical displacement is presented as a dashed line, (c) 0.25 strain, all rate cases, and (d) 0.50 strain, all rate cases.

This heterogeneity (i.e. normal and shear strain combinations) cannot be readily reproduced in 2-D systems, and thus the 3-D CSD may provide an intermediate level of complexity between 2-D and in or ex vivo models.

3.2. Acellular characterization of displacement

Characterization of the microbead displacement throughout the acellular gel construct indicated that the beads followed a linear path regardless of the strain magnitude or strain rate (Fig. 5). In order to obtain a complete set of images throughout the 3-D structure it was necessary to use a strain-and-hold method, rather than the short dwell time used for the cell experiments. The slopes of the lines were statistically the same for a given strain magnitude and therefore these conditions were combined. Displacements in the horizontal plane (x_1,x_2) were measured based on linear deformation, where vertical displacement (x_3 direction) was minimal (<5 μm, which is within 2% of the maximum x_2 displacement) and therefore was considered to be zero, validating the theoretical assumption. The bead displacement in the x_2 direction was dependent on the shear angle and the vertical position within the gel. Further regression analysis revealed that there was a difference between the measured paths and theoretical simple shear strain ($p<0.01$), indicating that the shear strain field is complex and likely contains elements of both simple and pure shear. However, if there is an

assumption of no-slip at the bottom plate (i.e., forcing the experimental x_3 intercept to zero) the slopes of the measured and theoretical shear strain profiles are statistically the same for the 0.25 strain cases ($p > 0.2$), indicating a better approximation for simple shear for the lower of the strain magnitudes tested.

3.3. Cell viability following 3-D shear strain in astrocytes and neurons

The 3-D astrocyte cultures were subjected to four combinations of strain and strain rate as described in Section 2. Astrocyte viability at 24 h after the insult was statistically lower for both strain magnitudes at the high strain rate ($20\,s^{-1}$) than either the unstrained controls (sham or naïve) or the quasistatic case ($p < 0.001$) (Fig. 6). There was no significant difference in cell viability between the low strain rate ($1\,s^{-1}$; quasistatic conditions) and the sham or naïve controls. In addition, there was no difference between the 0.25 strain and 0.50 strain levels for either the quasistatic or high strain rate cases, suggesting that these cells are not sensitive to the level of strain for the magnitudes tested (Fig. 6). Neurons subjected to high strains at two different rates ($20\,s^{-1}$ and $30\,s^{-1}$) were both injured more than sham or naïve controls ($p < 0.001$) at 24 h post-deformation, demonstrating that this system is capable of injuring more than one type of neural cell (Fig. 7). There were no significant differences in viability between astrocytes and neurons compared under matched conditions (naïve or sham cases) indicating consistent baseline viability for these cells types. Furthermore, there was not a significant difference in the injury response between these cell types at a matched strain regime (0.50 strain, $20\,s^{-1}$ strain rate).

3.4. Neurite orientation following 3-D shear strain in neurons

The distribution of neurites within 3-D neuronal cultures was examined after high strain, high strain rate injury (0.50, $30\,s^{-1}$) in order to assess whether neurite

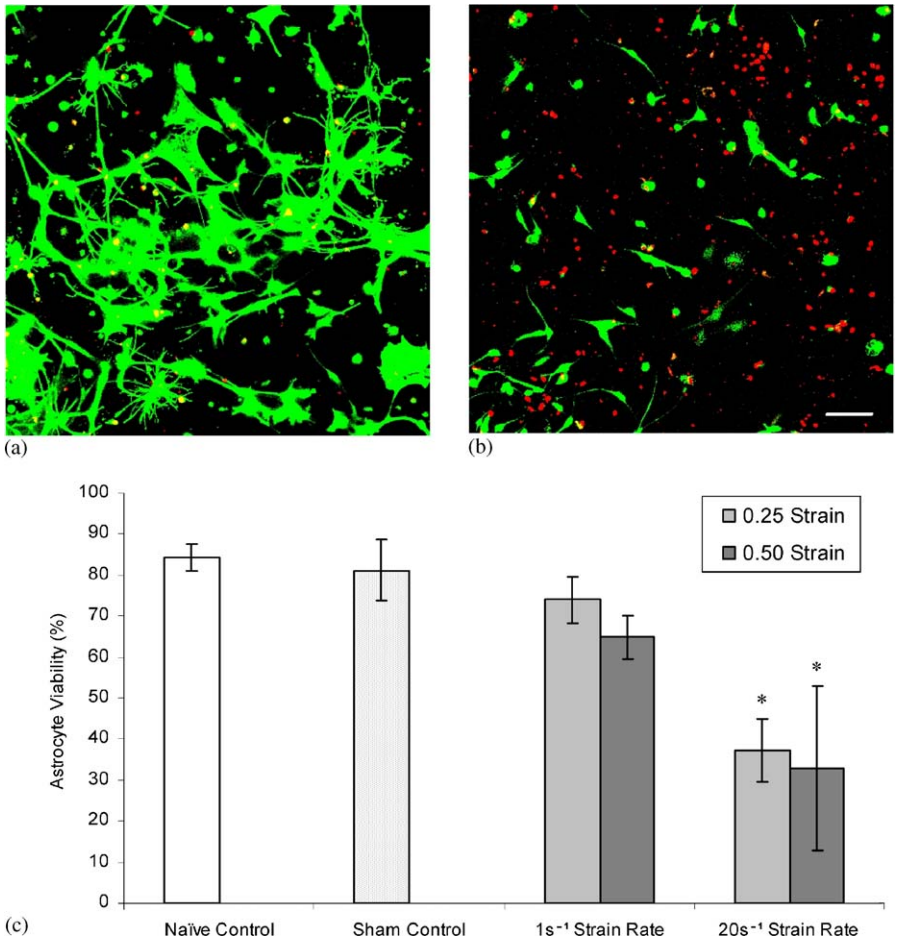

Fig. 6. Astrocyte viability following deformation. 3-D astrocyte cultures were stained with calcein AM (labeling live cells green) and EthD-1 (labeling nuclei of dead cells red) at 24 h post-loading or sham conditions. Representative confocal reconstructions of (a) sham culture and (b) culture subjected to 0.50 strain, $20\,s^{-1}$ strain rate (scale bar = 100 μm). (c) There was a significant decrease in astrocyte viability after high rate loading with the 3-D CSD (*, $p < 0.001$), but this change in viability was not dependent on strain magnitude. Error bars represent standard deviation.

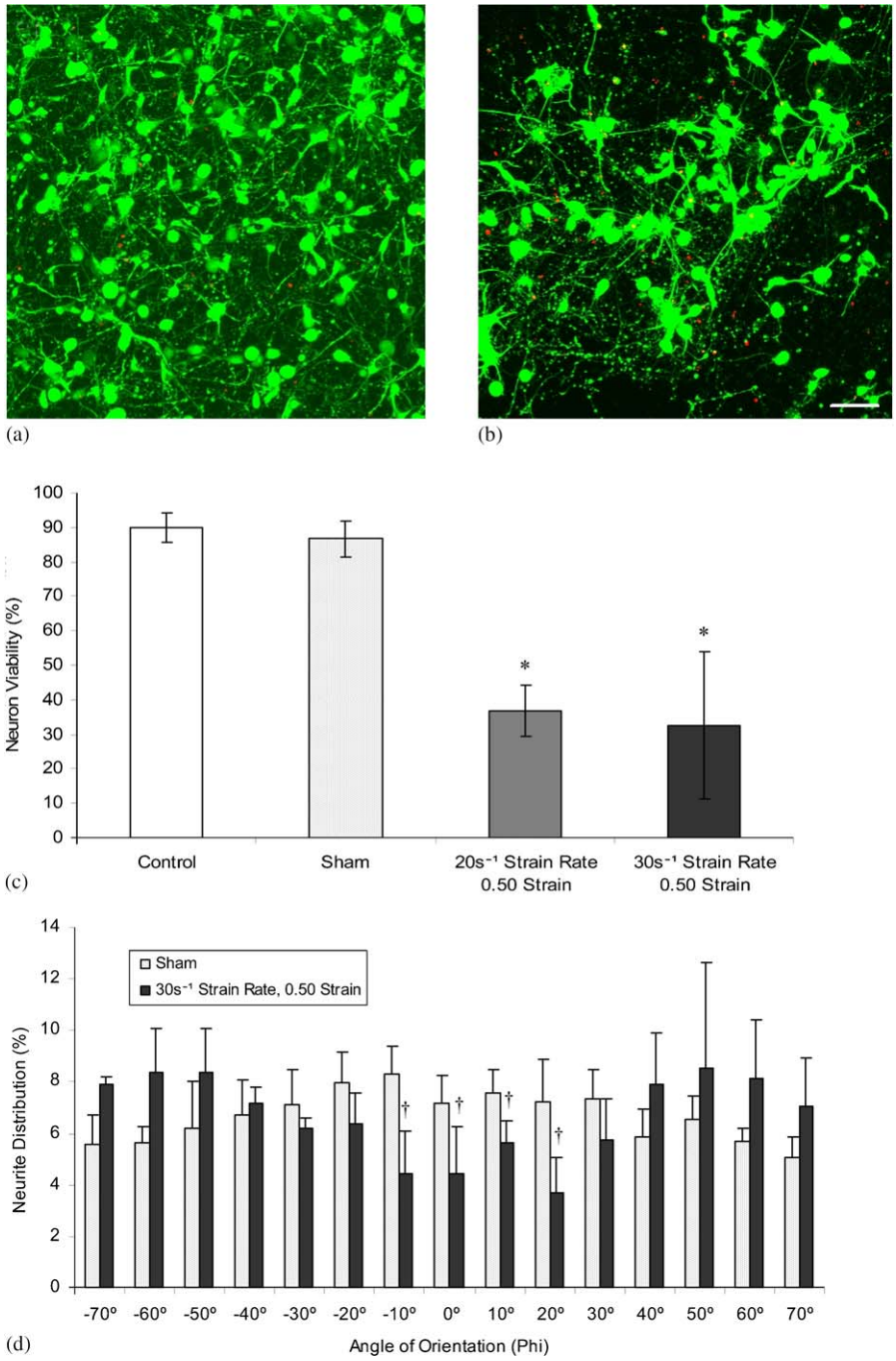

Fig. 7. Neuron viability and neurite distribution following deformation. Confocal reconstructions of 3-D neuronal cultures at 24 h post-loading or sham conditions. Live cells are stained green and the nuclei of dead cells are stained red for (a) sham culture and (b) culture loaded at 0.50 strain, $30\,s^{-1}$ strain rate (scale bar = 50 μm). (c) There was a significant decrease in neuronal viability versus sham for both loading regimes evaluated with neuronal cultures (*, $p<0.001$). (d) The distribution of neurites for sham cultures was compared to the distribution of neurites remaining after loading at 0.50 strain, $30\,s^{-1}$ strain rate. There was a significant reduction in the percent of total neurites at angles of orientation (ϕ, the projected neurite orientation in the x_3,x_2 plane) close to the horizontal plane (†, $p<0.05$), correlating with orientations predicted to experience maximum axial-shear strain (E'_{23}). Error bars represent standard deviation.

orientation within the culture, and hence varying strain combinations, contributed to severity of cell injury. The number of neurites per plane across all orientation angles was lower in injured cultures (15.4 ± 9.0) versus sham conditions (45.1 ± 19.6) (mean ± SD). The percent of neurites per orientation angle (corresponding to ϕ, the projected angle in the x_3,x_2 plane) after injury was compared to the neurite distribution found in neurons subjected to sham conditions at corresponding orientation angles. After high strain, high strain rate injury

there was a significant loss of neurites ($p<0.05$) at orientation angles of −10, 0, 10, and 20 degrees (representing ϕ), which is indicative of degeneration and subsequent cell death (Schwab and Bartholdi, 1996; Sievers et al., 2003) (Fig. 7d). These angles bracket the range at which axial-shear strain (E'_{23}) is the highest (see Fig. 4f), suggesting that strain combinations are important to cellular response in a dynamic loading regime. This pattern of preferential neurite loss signifies the need to consider cell orientation as a factor for response to mechanical stimuli in 3-D configurations.

4. Discussion

We have designed a device that is capable of mechanically deforming 3-D neural cell cultures and demonstrated its use as a quantifiable, reproducible model of in vitro traumatic injury. A shear deformation was achieved through the parallel motion of the top plate of a cell chamber with respect to the bottom surface, thus uniformly deforming the 3-D cell culture. A linear shear strain field for several combinations of strain and strain rate was determined using microbead tracking, illustrating the ability of this system to simulate shear strain—the deformation pattern associated with diffuse brain injury (Chu et al., 1994; Donnelly and Medige, 1997; Holburn, 1943). The extent of matrix deformation is controlled and therefore the cell response can be correlated to loading parameters. We showed that cell death in astrocytes and neurons was dependent on a combination of high strain and strain rate providing evidence that the mode of loading is important to the validation of cell injury systems.

Measuring the displacement of fluorescent microbeads revealed deviations from the simple shear assumption, with mean regression slopes of the measured paths consistently approximately 20% lower than the theoretical slopes. While an explanation of these differences may be explained by slight rotation of the culture (i.e. an underestimation of γ), vertical displacement of the beads was less than 2% of the x_2 displacement, indicating that the confinement of the system limits rotation of the culture. Strain patterns within the culture are complex and these results suggest that elements of both pure and simple shear may be present in this system. The strain profile at 0.25 strain was shown to be a better approximation of simple shear than the 0.50 case, suggesting that larger displacement angles may lead to deviation from the theoretical simple shear strain. In addition, based on finite deformation theory, the application of traction forces at the end faces may be required for a true simple shear deformation. Because the Matrigel was contained in an elastic Sylgard mold, the motion was constrained and dictated by the overall displacement of the mold. The forces at the end faces, however, are governed by the attachment of the Sylgard mold to the Matrigel and, while the matrix is contained, during dynamic loading we cannot rule out the possibility that nonuniform forces result from the bulk deformation that may result in a variation from ideal simple shear. This characterization over a range of input parameters, however, served to demonstrate that the CSD consistently induces the prescribed deformation in a linear manner and that we can use a theoretical analysis to approximate the complex strain patterns within the 3-D culture.

We demonstrated that the 3-D CSD is capable of injuring both primary cortical astrocytes and neurons in a 3-D configuration. This study correlates with previous studies on neural or neural-like cultures, in that magnitude and rate of mechanical deformation are determinants in cellular outcome (Cargill and Thibault, 1996; Ellis et al., 1995; LaPlaca and Thibault, 1997; Morrison et al., 1998a, b). No difference between cellular response for the injured astrocytes was detected at the 0.25 strain and 0.50 strain cases at the high strain rate. This may indicate that at the $20\,s^{-1}$ strain rate, maximum cell death occurs below the 0.25 strain level. Alternatively, cell death may be strain magnitude independent for this rate tested. Similarly, although high rate loading of neurons resulted in significant cell death, there was no difference between the two rates tested, suggesting a rate threshold in the cellular response. Moreover, the 3-D CSD is capable of eliciting cellular responses under a range of loading conditions, thus allowing for the investigation of cellular thresholds.

In contrast to 2-D injury models, the current 3-D configuration may lead to increased heterogeneity of strains at the cellular level. A uniform distribution of cells within a largely isotropic 3-D matrix results in a corresponding distribution of neurite orientations with respect to the horizontal plane, and therefore a wider range of local cellular strain for the same bulk shear deformation. The results of the theoretical strain analysis of this system show that cells with a 3-D orientation within the shear field experience alternate combinations of normal and shear deformation, and overall higher magnitudes of deformation than cells in a planar geometry. We demonstrated that these combinations of strain, and in particular high shear strain, may preferentially contribute to cell death. The assumption was made that neurite orientation at the time of loading or sham conditions was represented by neurite orientation assessed 24 h later. While it is possible that some degree of network re-organization may occur following mechanical trauma, we do not observe any soma or neurite movement in this system at this time point, as may be the case in different cell types. Overall, the heterogeneity of the strain field as a function of cellular orientation may be further exploited to investigate the

effect of various combinations of normal and shear strains on cellular response.

While 3-D cultures exposed to shear strain may have a non-uniform strain field at the cellular level, other features of the system may contribute to the response. For example, 3-D cultures may be more susceptible to secondary injury cascades than 2-D models due to the altered mass transport properties of the 3-D configuration. The high ratio of extracellular to intracellular volume in 2-D cultures and the sink-like property of the bathing medium may serve to dilute secreted or released molecules at the time of injury. Thus, a 3-D configuration with more physiologically relevant cell-cell interactions (Gumbiner and Yamada, 1995; Schmeichel and Bissell, 2003) may provide a setting in which to investigate of the role of autocrine and paracrine signaling in response to mechanical trauma. The injury response may be exacerbated by the moderate level of baseline cell death in the 3-D astrocyte cultures. Astrocytes cultured in 3-D may require perfusion or more frequent media changes in order to maintain optimal health due to their proliferative capability as compared to non-dividing cells. In addition, different cell types may respond differently to the microenvironment and properties of the surrounding matrix (Flanagan et al., 2002). However, after high strain, high strain rate loading, similar levels of cell death were observed in both astrocytes and neurons, demonstrating the ability of the 3-D CSD to injure neural cells cultured in 3-D.

To our knowledge, this is the first report of a biomechanically controlled traumatic injury model using 3-D cultures. This 3-D model produces cellular deformation in a more in vivo-like configuration than traditional monolayers, but still provides the benefit of the absence of systemic factors. The deformation rates and magnitudes that were used in this study are in the range of those that occur in inertial human head injuries (Gennarelli et al., 1982; Margulies and Thibault, 1992; Margulies et al., 1990). This model will aid in elucidating the complex biochemical and molecular cascades that occur after a traumatic insult and may be used to investigate a wide range of shear loading profiles in a variety of cell types. Biomechanically characterized in vitro models such as the 3-D CSD, used in combination with animal models and computer simulations, will lead to a better understanding of TBI and positively impact the development of treatment strategies.

Acknowledgements

Funding for this study was partially provided by the NSF (CAREER Award to ML, BES-0093830) and the NIH (EB001014-2). The authors also acknowledge Maggie Wolfson (GT, Department of Biomedical Engineering) for technical assistance in image analysis.

References

Balentine, J.D., Greene, W.B., Bornstein, M., 1988. In vitro spinal cord trauma. Laboratory Investigation 58 (1), 93–99.

Cargill, R.S., Thibault, L.E., 1996. Acute alterations in $[Ca^{2+}]_i$ in NG108-15 cells subjected to high strain rate deformation and chemical hypoxia: an in vitro model for neural trauma. Journal of Neurotrauma 13 (7), 395–407.

Chu, C.S., Lin, M.S., Huang, H.M., Lee, M.C., 1994. Finite element analysis of cerebral contusion. Journal of Biomechanics 27 (2), 187–194.

Cukierman, E., Pankov, R., Stevens, D.R., Yamada, K.M., 2001. Taking cell-matrix adhesions to the third dimension. Science 294 (5547), 1708–1712.

Cukierman, E., Pankov, R., Yamada, K.M., 2002. Cell interactions with three-dimensional matrices. Current Opinion in Cell Biology 14 (5), 633–639.

Donnelly, B.R., Medige, J., 1997. Shear properties of human brain tissue. Journal of Biomechanical Engineering 119 (4), 423–432.

Ellis, E.F., McKinney, J.S., Willoughby, K.A., Liang, S., Povlishock, J.T., 1995. A new model for rapid stretch-induced injury of cells in culture: characterization of the model using astrocytes. Journal of Neurotrauma 12 (3), 325–339.

Fawcett, J.W., Housden, E., Smith-Thomas, L., Meyer, R.L., 1989. The growth of axons in three-dimensional astrocyte cultures. Developmental Biology 135 (2), 449–458.

Fawcett, J.W., Barker, R.A., Dunnett, S.B., 1995. Dopaminergic neuronal survival and the effects of bFGF in explant, three dimensional and monolayer cultures of embryonic rat ventral mesencephalon. Experimental Brain Research 106, 275–282.

Flanagan, L.A., Ju, Y.E., Marg, B., Osterfield, M., Janmey, P.A., 2002. Neurite branching on deformable substrates. Neuroreport 13 (18), 2411–2415.

Geddes, D.M., Cargill II, R.S., 2001. An in vitro model of neural trauma: device characterization and calcium response to mechanical stretch. Journal of Biomechanical Engineering 123 (3), 247–255.

Gennarelli, T.A., 1993. Mechanisms of brain injury. Journal of Emergency Medicine 11 (Suppl 1), 5–11.

Gennarelli, T.A., 1994. Animate models of human head injury. Journal of Neurotrauma 11, 357–368.

Gennarelli, T.A., Thibault, L.E., Adams, J.H., Graham, D.I., Thompson, C.J., Marcincin, R.P., 1982. Diffuse axonal injury and traumatic coma in the primate. Annals of Neurology 12 (6), 564–574.

Granet, C., Laroche, N., Vico, L., Alexandre, C., Lafage-Proust, M.H., 1998. Rotating-wall vessels, promising bioreactors for osteoblastic cell culture: comparison with other 3D conditions. Medical and Biological Engineering and Computing 36 (4), 513–519.

Gross, G.W., Lucas, J.H., Higgins, M.L., 1983. Laser microbeam surgery: ultrastructural changes associated with neurite transection in culture. The Journal of Neuroscience 3 (10), 1979–1993.

Gumbiner, B.M., Yamada, K.M., 1995. Cell-to-cell contact and extracellular matrix. Current Opinion in Cell Biology 7 (5), 615–618.

Holburn, A.H., 1943. Mechanics of head injuries. Lancet 2, 438–441.

LaPlaca, M.C., Thibault, L.E., 1997. An in vitro traumatic injury model to examine the response of neurons to a hydrodynamically induced deformation. Annals of Biomedical Engineering 25 (4), 665–677.

Lucas, J.H., Gross, G.W., Emery, D.G., Gardner, C.R., 1985. Neuronal survival or death after dendrite transection close to the perikaryon: correlation with electrophysiologic, morphologic, and ultrastructural changes. Central Nervous Systems Trauma 2 (4), 231–255.

Margulies, S.S., Thibault, L.E., 1992. A proposed tolerance criteria for diffuse axonal injury in man. Journal of Biomechanics 25 (8), 917–923.

Margulies, S.S., Thibault, L.E., Gennarelli, T.A., 1990. Physical model simulations of brain injury in the primate. Journal of Biomechanics 23 (8), 823–836.

Morrison, B.R., Meaney, D.F., McIntosh, T.K., 1998a. Mechanical characterization of an in vitro device designed to quantitatively injure living brain tissue. Annals of Biomedical Engineering 26 (3), 381–390.

Morrison, B.R., Saatman, K.E., Meaney, D.F., McIntosh, T.K., 1998b. In vitro central nervous system models of mechanically induced trauma: a review. Journal of Neurotrauma 15 (11), 911–928.

Mukhin, A., Fan, L., Faden, A.I., 1996. Activation of metabotropic glutamate receptor subtype mGluR1 contributes to post-traumatic neuronal injury. Journal of Neuroscience 16 (19), 6012–6020.

Murphy, E.J., Horrocks, L.A., 1993. A model for compression trauma: pressure-induced injury in cell cultures. Journal of Neurotrauma 10 (4), 431–444.

Ogden, R.W., 1984. Non-linear Elastic Deformations. Halsted Press, New York, 532pp.

Ommaya, A.K., Thibault, L., Bandak, F.A., 1994. Mechanisms of impact head injury. International Journal of Impact Engineering 15 (4), 535–560.

Regan, R.F., Choi, D.W., 1994. The effect of NMDA, AMPA/kainate, and calcium channel antagonists on traumatic cortical neuronal injury in culture. Brain Research 633, 236–242.

Roberts, I., Schierhout, G., Alderson, P., 1998. Absence of evidence for the effectiveness of five interventions routinely used in the intensive care management of severe head injury: a systematic review [see comments]. Journal of Neurology, Neurosurgery and Psychiatry 65 (5), 729–733.

Schmeichel, K.L., Bissell, M.J., 2003. Modeling tissue-specific signaling and organ function in three dimensions. Journal of Cell Science 116 (Part 12), 2377–2388.

Schwab, M.E., Bartholdi, D., 1996. Degeneration and regeneration of axons in the lesioned spinal cord. Physiological Review 76 (2), 319–370.

Shepard, S.R., Ghajar, J.B.G., Giannuzzi, R., Kupferman, S., Hariri, R.J., 1991. Fluid percussion barotrauma chamber: a new in vitro model for traumatic brain injury. Journal of Surgical Research 51, 417–424.

Shuck, L.Z., Advani, S.H., 1972. Rheological response of human brain tissue in shear. Journal of Basic Engineering 905–911.

Sieg, F., Wahle, P., Pape, H.-C., 1999. Cellular reactivity to mechanical axonal injury in an organotypic in vitro model of neurotrauma. Journal of Neurotrauma 16 (12), 1197–1213.

Sievers, C., Platt, N., Perry, V.H., Coleman, M.P., Conforti, L., 2003. Neurites undergoing Wallerian degeneration show an apoptotic-like process with Annexin V positive staining and loss of mitochondrial membrane potential. Neuroscience Research 46 (2), 161–169.

Takeshita, K., Bowen, W.C., Michalopoulos, G.K., 1998. Three-dimensional culture of hepatocytes in a continuously flowing medium. In Vitro Cellular and Development Biology-Animal 34 (6), 482–485.

Tecoma, E.S., Monyer, H., Goldberg, M.P., Choi, D.W., 1989. Traumatic neuronal injury is attenuated by NMDA antagonists. Neuron 2 (6), 1541–1545.

Wallis, R.A., Panizzon, K.L., 1995. Felbamate neuroprotection against CA1 traumatic neuronal injury. European Journal of Pharmacology 294 (2–3), 475–482.

Wang, F., Weaver, V.M., Petersen, O.W., Larabell, C.A., Dedhar, S., Briand, P., Lupu, R., Bissell, M.J., 1998. Reciprocal interactions between beta1-integrin and epidermal growth factor receptor in three-dimensional basement membrane breast cultures: a different perspective in epithelial biology. Proceedings of the National Academy of Science USA 95 (25), 14821–14826.

Yamada, K.M., Pankov, R., Cukierman, E., 2003. Dimensions and dynamics in integrin function. Brazilian Journal of Medical and Biological Research 36 (8), 959–966.